Variability Studies of Multi-wavelength Data from gamma-ray Blazars Mrk 421 and Mrk 501

Brandon Becker

August 12, 2014

Abstract

In this thesis we take astronomical multi-wavelength data from nearby blazars Markarian 421 and Markarian 501 and perform computational analysis and correlative studies to determine any possible time lag across different bands of our targets as well as to measure the statistical significance of this calculated result. The data was taken over the interval of December 2010 to May 2012 from multiple instruments spanning a broad range of wavelengths. We used the Discrete Correlation Function (DCF) to determine the time lag factor across data set pairs, focusing on X-ray and Very-High-Energy (VHE; >100 GeV) data. To establish the significance of any correlations found this way, we create Monte Carlo data sets matching the parameters from each light curve's power spectrum distribution, and compare results to our original data. The calculated time lag for Markarian 421 is 2 ± 5 days, consistent with our originally hypothesized zero time lag, indicating the dominant emission process for this target is synchrotron self-compton (SSC). Markarian 501's data provides less resolution but also contains zero time lag within its range of error, consistent with our expectation.

1 Introduction

It is believed that at the center of almost every galaxy exists a supermassive black hole. Once a black hole has achieved about 10^6 solar masses it is considered to be supermassive. These singularities bend space and time to the degree that not even light can escape their gravitational influence. Stellar black holes occur as a result of the collapse of a massive star at the end of its life cycle, and some of them become the seeds that give origin to the supermassive class through the continuous accretion and merging of small black holes through the galaxy's history. Black holes located the densely populated center of a galaxies are known to ingest up to hundreds of solar masses a day through a process called accretion [11]. In normal galaxies, emissions are dominated by thermal processes such as thermal radio emissions and infrared from the heated interstellar dust. In the other hand, objects which exhibit powerful accretion are given the label of Active Galactic Nuclei (AGN). In this case the emission is dominated by non-thermal

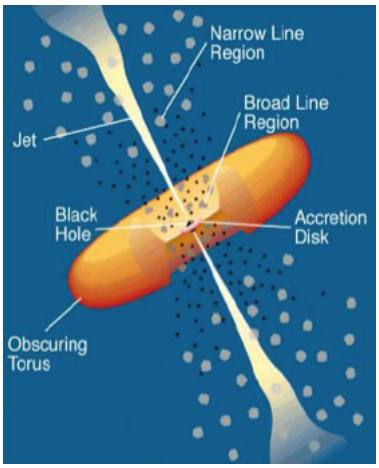

Figure 1: Schematic of a typical AGN with jets, from [11].

processes. In the study and interpretation of the variability in these processes we hope to provide additional insight toward the mechanisms responsible for these emissions [4].

1.1 Active Galactic Nuclei and Blazars

AGN are usually divided in classes and subclasses according to their properties [11]. The most common of these being a Seyfert galaxy. These have low radio emission nuclei and have high-ionization emission lines. Seyferts are divided into type I and type II, type I belonging to those with a broad emission line imposed upon a narrow emission line, implying large doppler shifts due to relativistic effects. The less luminous type II display primarily narrow emission lines. The distinction between these can be linked to the orientation of the galaxy relative to us, Type I having its accreting plane perpendicular to earth, thus exposing gas clouds orbiting the center with high velocity, producing thus the broadened lines. Type II is typically edge on, with the outer galactic structure blocking most of the Doppler broadened emission bands, however the torus of light escaping the bulge illuminates any plasma above and below the galactic plane. This is shown schematically in Figure 1.

Quasars (quasi-stellar objects) are the second largest subset, and are bluish in color and have strong optical emissions which are misleadingly star-like in appearance. They are distinct from Seyferts in being unresolved in optical observations, with few exceptions and only when using the most powerful telescopes. We now know that these quasars are hosted in elliptical galaxies, which supports the idea that the dissolution of the spiral structure into an elliptical shape due to a merger with another galaxy. The subsequent accretion of interstellar debris in large quantities at the center fuels the powerful emissions of the supermasive black hole. Quasars also fall into subsets of being either radio-quiet

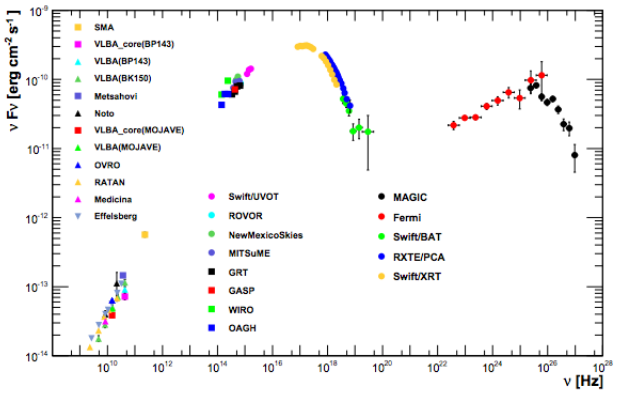

Figure 2: Spectral Energy Distribution (SED) of Markarian 421, from [1]. This very complete multi-wavelength spectrum shows the double peak feature that is typical of blazars: synchrotron photons (left peak) and high-energy photons (right peak).

or radio-loud, as well as being divided similarly to the difference in orientation of type I or type II Seyfert galaxies, broad emission line radio galaxies (BLRGs) and narrow-line radio galaxies (NLRGs) respectively.

Blazars are the most extreme subset of AGN: they are the brightest, the most variable and the most energetic, reaching individual photon energies of tens of Tera-electron Volts (1 TeV $= 10^{12}$ eV). Blazars are quasars with their jets oriented at Earth, making these relativistic energies possible through Doppler boosting effects. A jet is an outbound stream of plasma ejected perpendicular to the plane of the galaxy hosting the accretion disk. Blazars are characterized by their rapid variability and polarized light. Of particular interest is the BL Lac type of blazars, which show no emission lines as opposed to Flat-Spectrum Radio Quasars (FSRQs), which produce strong emission lines.

1.2 Physics of Blazar Emissions

From radio observations we know that much of the light produced in these objects at long wavelengths (radio to optical, and sometimes x-rays) is due to synchrotron radiation. As charged particles move through magnetic fields, they emit polarized light known as cyclotron radiation (for the machine where the phenomena was first observed). At relativistic velocities, it is referred to as synchrotron radiation. Understanding the mechanisms accelerating these particles to very high energies, the origin and structure of these large magnetic fields, and how everything relates to the black hole are some of the most important questions in astrophysics.

1.2.1 Synchrotron Self-Compton (SSC) Model

Light is known to scatter off matter in an effect known as Compton Scattering. With relativistic ions such as the electrons and positrons available with very high energies in the plasma jets of a blazar, an effect known as Inverse Compton allows for photons to scatter off these leptons and gain energy. In the Synchrotron Self-Compton model, the outgoing jets of relativistic leptons produce synchrotron radiation in the presence of the magnetic field produced by the blazar, which we observe as optical through x-ray photons depending on the blazar. These photons can scatter to higher energies off the same population of electrons that producedthem in the same place. An increase in the number of leptons present would also increase the photons available to scatter, therefore we expect a quadratic correlation between gamma-ray and X-Ray photons in the SSC scenario.

1.2.2 External Compton Model

Clouds of ionized gas sometimes occupy the areas around the torus of the blazar. Photons radiated from these clouds illuminate the jet and just as in the Synchrotron Self-Compton model, are able to be scattered to gamma-ray energies. Unlike the SSC model, the external compton model requires a linear correlation of leptons to high-energy photons, as the supply of available photons is independent of the electrons. Therefore, an increase in the population of jet electrons, will have a linear correlation with the relative flux of gamma rays.

1.2.3 Hadronic Model

Heavier particles dissipate less power to synchrotron radiation, thus allowing them to reach higher energies more efficiently given the same acceleration parameters. The hadronic model proposes that ultra-relativistic protons are able to reach energies such that the synchrotron radiation they produce reaches all the way to gamma-ray energies. Another possibility for the hadronic model is the photo-pion decay in which a proton interacts with a photon producing a cascade of particles including pions, photons and neutrinos. This model is less favored compared to the leptonic models described above, and in this case we don't expect a clear correlation between low and high-energy photons.

1.3 Multi-Wavelength Observations

1.3.1 *Fermi*

Fermi is a space-based satellite launched June 11, 2008 as a gamma-ray imaging telescope [3]. Operated by NASA and a collaboration of international institutions, this multinational project was built with the mission to help further understand mechanisms of particle acceleration in AGN, supernova, search for evidence of dark matter, and to determine and resolve the sources of gamma

ray bursts. As the successor to the Energetic Gamma Ray Experiment Telescope (EGRET) launched in 1991, *Fermi* is composed of two instruments: the Large Area Telescope (LAT) is sensitive to individual photons in the energy range from 20 MeV to 300 GeV and due to its large field of view and rocking motion is able to cover the whole sky every 3 hours. The secondary instrument is the Gamma-Ray Burst Monitor (GBM), which is sensitive to photon energies between 15 keV and 30 MeV and observes from all directions not blocked by the Earth. The GBM detects and localizes gamma-ray bursts (GRB) within its large field of view and then provides prompt alerts to the LAT and to ground-based instruments.

1.3.2 VERITAS

The Very Energetic Radiation Imaging Telescope Array System (VERITAS) [2], is a ground-based, gamma-ray telescope located in the Fred Lawrence Whipple Observatory in Arizona. VERITAS detects Cherenkov radiation created from gamma-photons striking atoms in our atmosphere to detect the incident gamma ray, and is capable of observing energies up to 30 TeV. Completed in 2007, it is sensitive to energies higher to those observed by Fermi and has other complementary capabilities such as better angular resolution and larger effective area.

1.3.3 Swift-XRT

Swift is a space satellite launched in 2004 by NASA as a multinational project to detect Gamma-Ray Bursts (GRBs). Using momentum wheels to rapidly orient itself to observe a GRB, it then relays information of the burst to observers. Comprised of three instruments, the X-Ray Telescope (XRT) and Ultraviolet/Optical Telescope (UVOT) are both aligned with the Burst Alert Telescope (BAT) for observations in multiple wavebands. It captures the afterglow of many of the gamma ray bursts in optical and X-ray with hopes of determining the cause of these mysterious sources of very energetic photons. When not observing GRBs, SWIFT monitors astronomical sources such as well known blazars.

1.4 Markarian 421 and Markarian 501

Markarian 421 is one the nearest blazars to Earth and is the among the brightest TeV blazars in the night sky. Located in Ursa Major at a redshift of z = 0.0308, this BL Lac object is a source of gamma-ray photons. It was determined to be a source of very-high-energy (E>300 GeV) gamma-ray photons by the Whipple observatory in 1992[7]. In addition to its high energies, Mrk 421 also shows variability in the brightness on a relatively short timescale. Markarian 501 is another near Earth (z = 0.034) BL Lac blazar that also exhibits very-high-energy emission and rapid variability. With the use of the data from multiple satellites observing overlapping time intervals from these two similar targets we

investigate the potential correlations of these data series, find significance of such correlations and interpret the physics responsible for the observed trends in data.

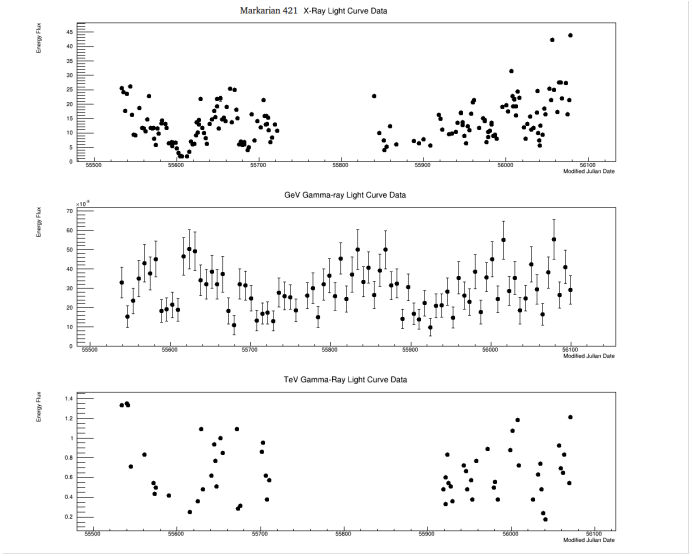

Figure 3: Markarian 421 Light Curve Data

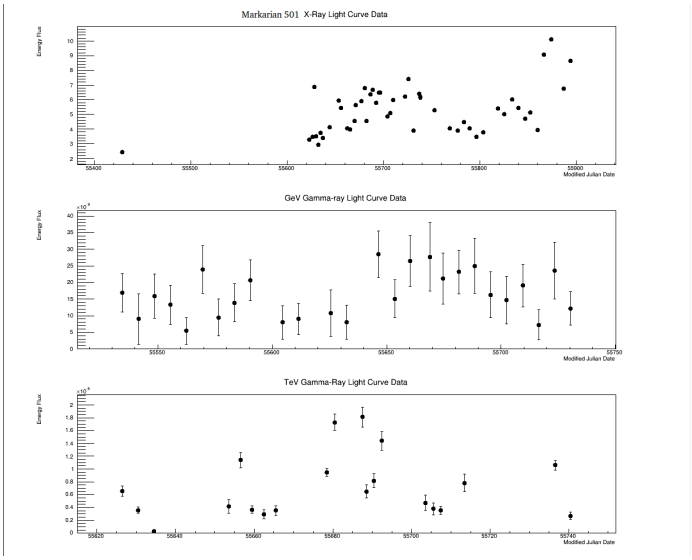

Figure 4: Markarian 501 Light Curve Data

1.5 Light Curve Data

The data that we use comes from the aforementioned instruments during the time interval spanning December 2010 to May 2012. The average relative flux was measured at times when the objects were visible during this interval. Observing the flux over time allows us to study the trends and correlations in the data set. The targets display the rapid variability and TeV energy that characterizes blazars.

2 Variability Studies

2.1 Motivation

As mentioned before, of the particular interest are the targets Mrk 421 and 501, these objects are excellent candidates for better understanding the physics of gamma-ray blazars. We investigate the variability and correlation among different wavelengths on the data shown in Figures 3 and 4.

2.2 Discrete Correlation Function

For two data sets measured in the same time interval but not simultaneously or regularly sampled one can use the Discrete Correlation Function (DCF) to find correlation between the two data sets [5]. Furthermore, this method allows us to find any time lag between possibly correlated bands such as X-rays and gamma rays. A correlation with negligible time lag implies that the same population of electrons that produce the synchrotron X-rays also scatter the TeV photons. A excessive time lag or lack of correlation would imply some different physics occurring where the X-ray production and gamma-ray production is occurring at two separate locations. Given a correlation, the Synchrotron Self-Compton model would also lead us to anticipate a quadratic correlation of TeV photons to X-Ray photons whereas an External Compton model would require a linear correlation.

2.3 Power Spectrum Distribution

Fourier transform analysis allow us to break down our data set into the frequency domain to observe the power spectral index of our light source [12]. A simple periodic process or combination of simple periodic processes would give us peaks of relative power occurring at their respective frequencies, and more complex sources give us a distribution of power over a range of frequencies. For stochastic processes such as those responsible for AGN variability we expect the power spectrum distributin (PSD) to follow a power law.

Our results are shown in Figures 5 and 6. All the obtained beta values (i.e. power law indices) were between values of 0 and -1, which is consistent with our expectations. This beta parameter allows us to later create simulated light curves that mimic the PSDs found for these blazars.

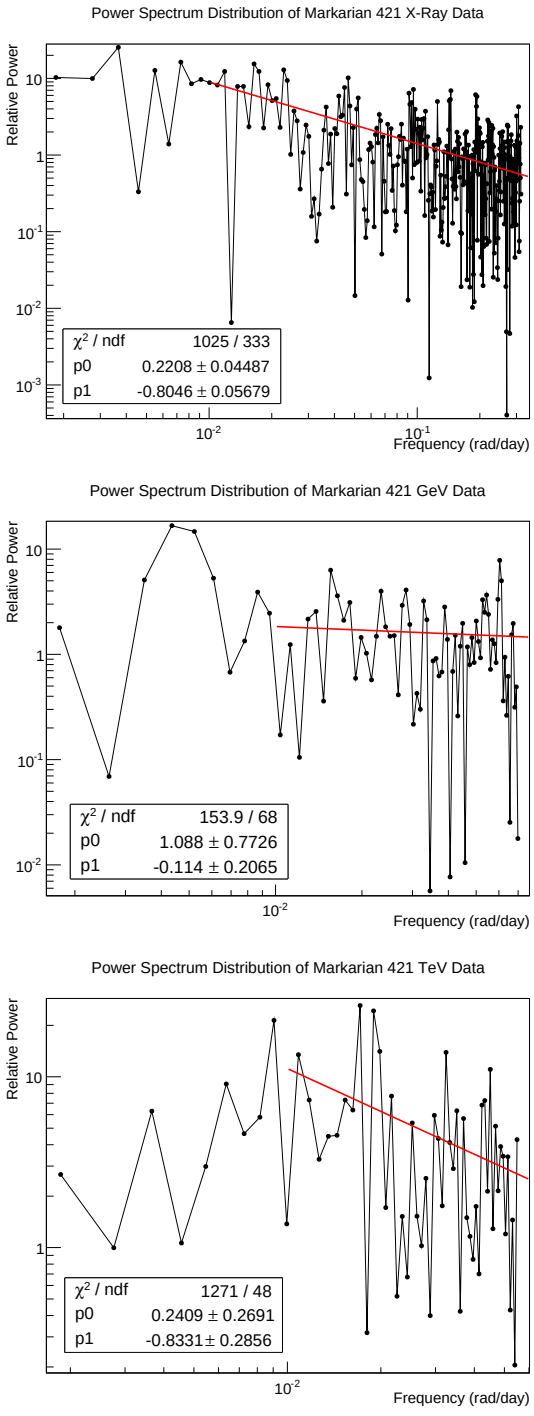

Figure 5: Markarian 421 PSD at x-ray energies (top), GeV energies (middle), and TeV energies (bottom).

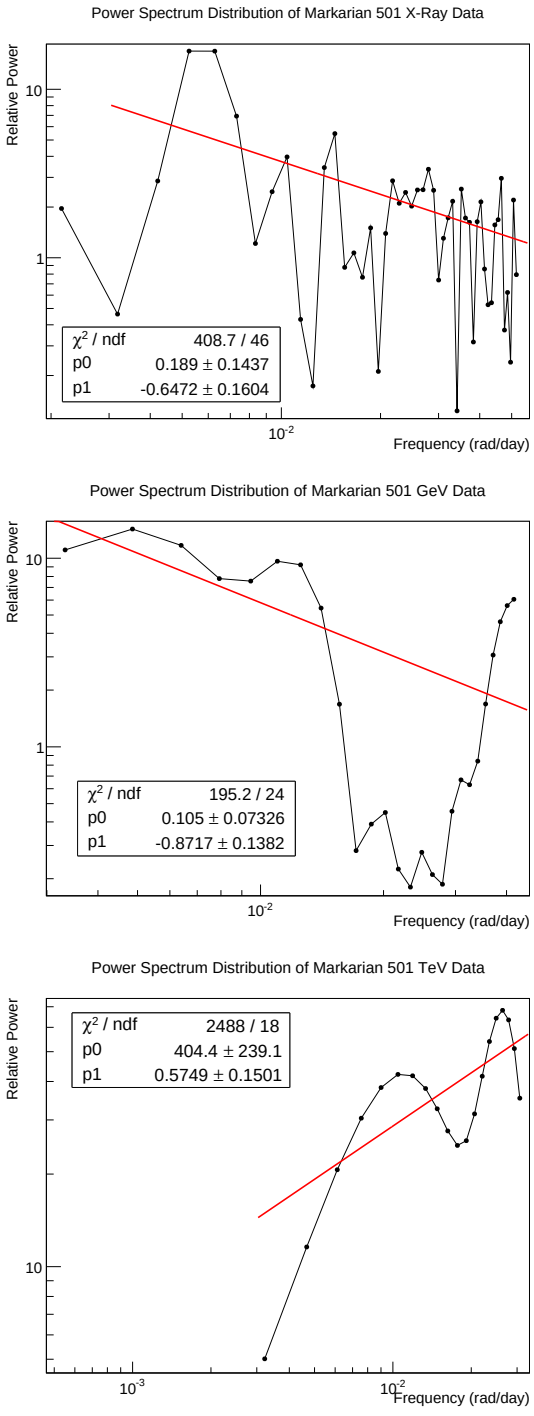

Figure 6: Markarian 501 PSD at x-ray energies (top), GeV energies (middle), and TeV energies (bottom).

Energy Band	Mrk 421	Mrk 501
X-ray	-0.80	-0.65
GeV	-0.11	-0.87
TeV	-0.83	0.575

Table 1: Power law fits to power spectrum distributions.

2.3.1 Discrete Correlation Functions Results

The DCF of both Markarian 421 and Markarian 501 for X-ray to TeV gives the best resolution of a peak centered about 0. X-ray to GeV and GeV to TeV data is less correlated (as is evident from Flux Correlation results below) and provide less conclusive support for the Synchrotron Self-Compton Model. However the peaks of the X-ray to TeV data which contain 0 within its error suggest that little if any time is occuring between a flare in X-ray and the accompanying TeV flare for both targets, which is supporting of the SSC model.

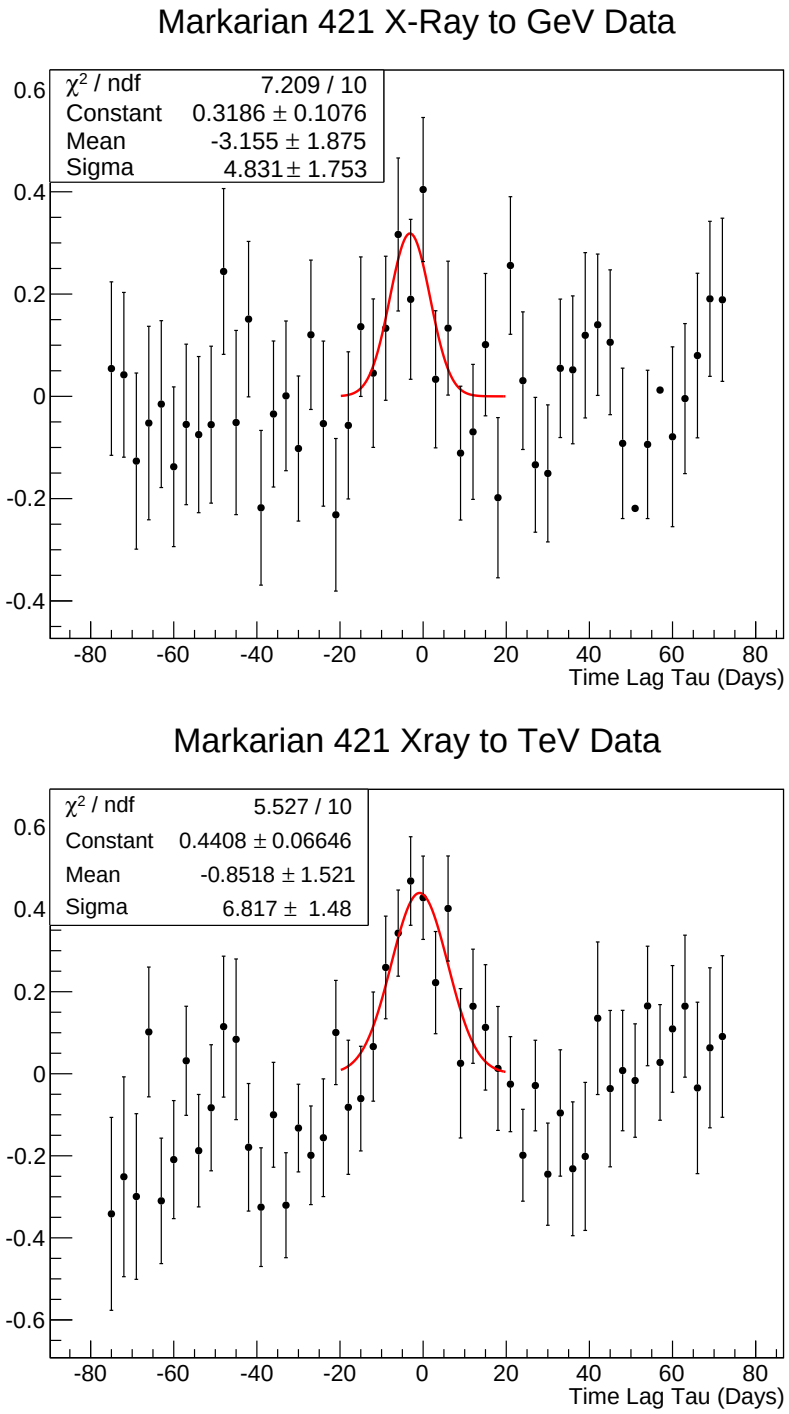

Figure 7: Markarian 421 discrete correlation functions (DCFs) for: x-ray vs GeV (top) and x-ray vs TeV (bottom)

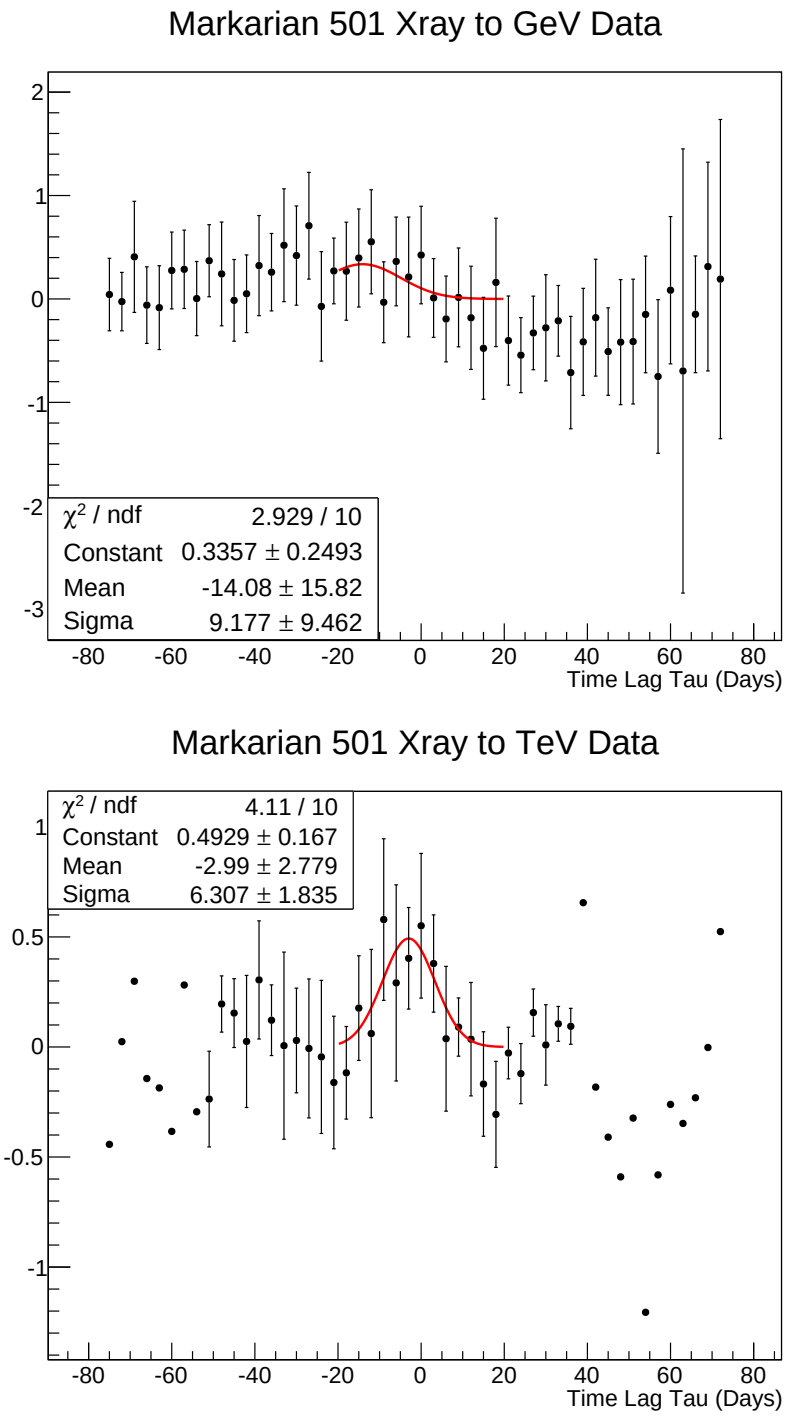

Figure 8: Markarian 501 discrete correlation functions (DCFs) for: x-ray vs GeV (top) and x-ray vs TeV (bottom)

2.3.2 Flux Correlation Results

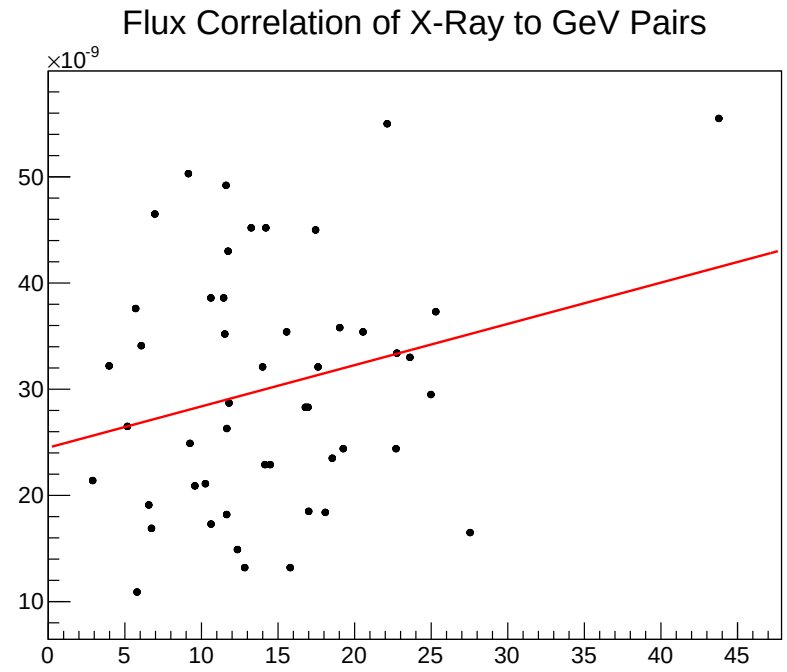

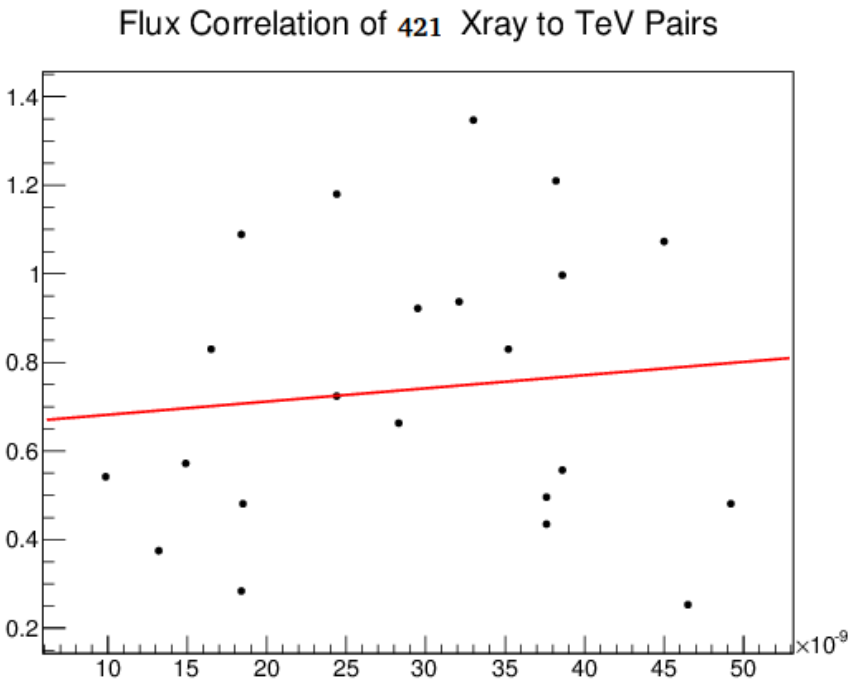

Figure 9: Markarian 421 correlation between x-ray flux and GeV flux (top), and x-ray flux vs TeV flux (bottom)

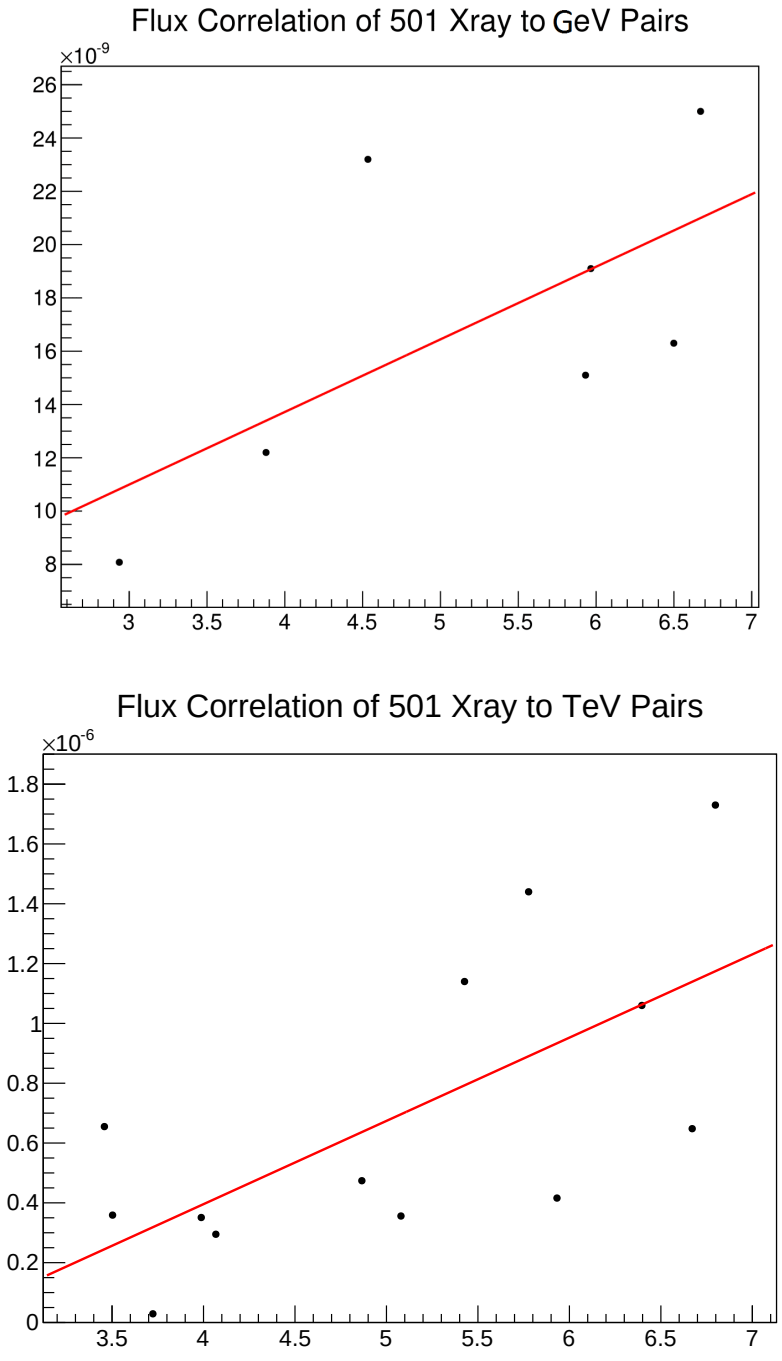

Figure 10: Markarian 501 correlation between X-ray flux and GeV flux (top), and X-ray flux vs TeV flux (bottom)

The observed correlation factor between X-ray and TeV data is 0.56 for Mrk 421 and 0.67 for Mrk 501. The correlation between X-ray to GeV and GeV to TeV data was weaker, and there were less contemporaneous pairs to draw a correlation from. The correlation factors provide further support for an Inverse Compton scenario, where the flux of gamma-rays is proportional to the number of X-rays available.

3 Monte Carlo Simulation

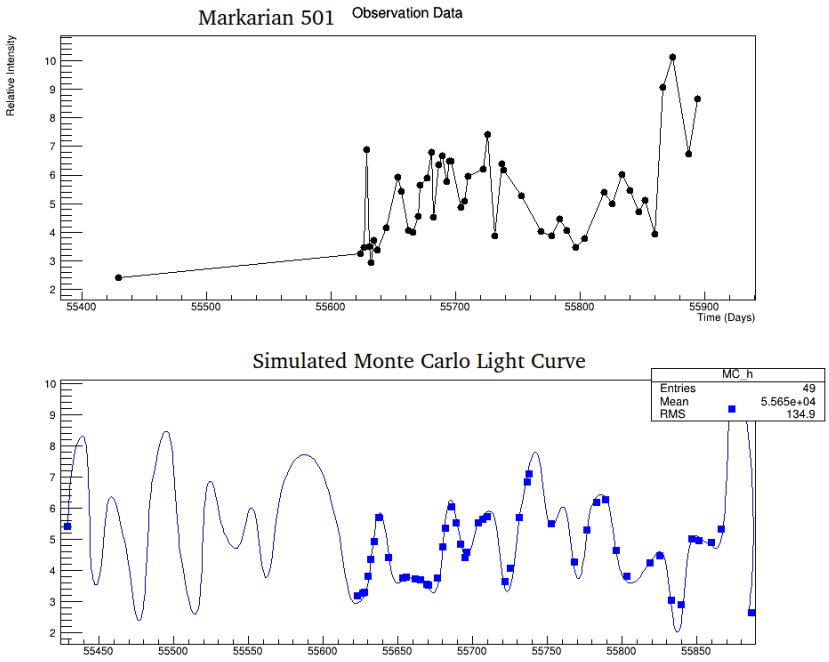

Figure 11: Simulated light curve of Mrk 501 based on PSD determined from the data.

3.1 Procedure

We start by obtaining the power spectrum index of our objects so that we can reconstruct a randomized light source that mimics the power spectrum distribution of our objects. We create a Power Spectrum Distribution and record the slope coefficient of the best fit to our data for X-ray, GeV, and TeV energy on both Markarian 421 and 501. Using the slope coefficient beta, we build an array of randomized complex numbers in the frequency domain. With our newly randomized complex data set we inverse fourier transform to the time interval in which the original observations were made and have a simulation light curve.

If we input two light curves of the same target, we can repeatedly compare the two simulated outputs and each pair will have a DCF and Flux Correlation.

3.2 Discrete Correlation Function and Flux Correlation Factor of Simulated Light Curves

In order to test the significance of the observed data set we calculate the DCF and flux correlation factor of each pair of simulated light curves. From each DCF, every bin's distribution of flux values is used to produce an average bin value as well as the standard deviation. Should the DCF of the original observation data fall outside the simulated light curves' variance we know that our observation is statistically significant. As per the flux correlations, two random light curves would have a random distribution of correlated pairs and the linear fit correlation factor would indicate little to no correlation. The observed light curves demonstrate a stronger correlation than the randomized light curves.

3.3 Results for DCF and Flux Correlation

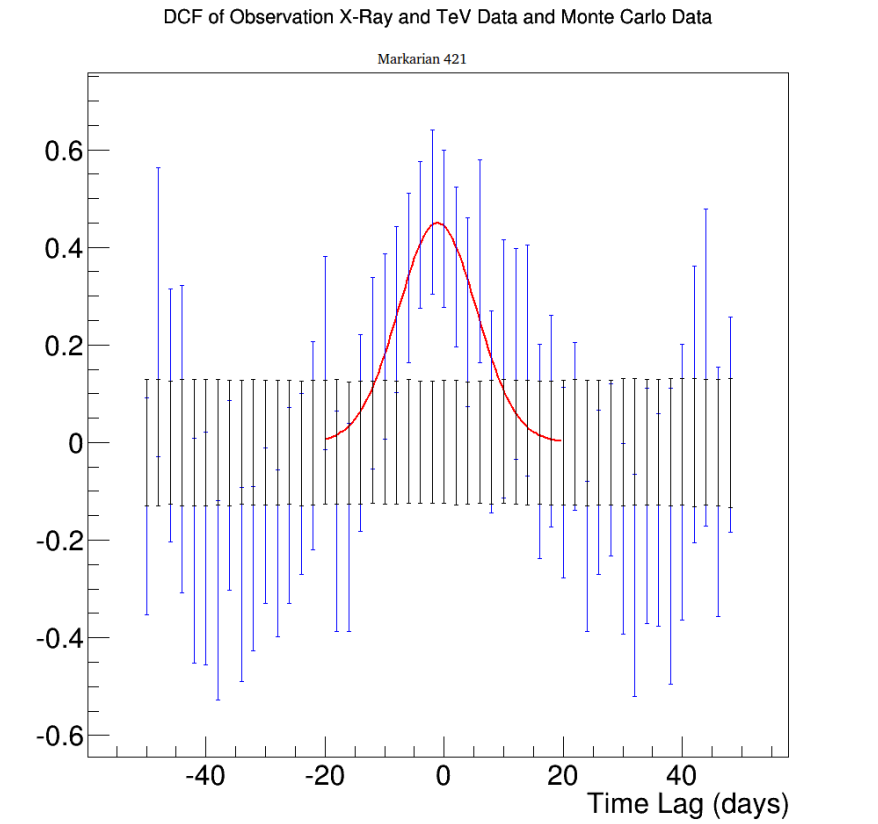

Figure 12: Mrk 421: DCF for data (blue points) and MonteCarlo light curves (shown as the average of 1000 curves and their RMS). The peak at a time lag of zero days is evidently not a statistical fluctuation.

Mrk 421	R_{MC}	$\sigma_{R_{MC}}$	R
X-ray vs TeV	0.00095	0.2485	0.5602
X-ray vs GeV	-0.0011	0.1063	0.249
GeV vs TeV	-0.0023	0.498	0.108
Mrk 501	R_{MC}	$\sigma_{R_{MC}}$	R
X-ray vs TeV			0.6732
X-ray vs GeV	0.005	0.448	0.6535
GeV vs TeV			0.2402

Table 2: Mean correlation factor R_{MC} and its standard deviation $\sigma_{R_{MC}}$ found for the Monte Carlo light curves compared to the values obtained from the data (R). Given these results, the correlation between X-ray and TeV is significant for the X-ray vs TeV and X-ray vs GeV light curves, as expected in leptonic models.

The graphs of the DCFs indicate that the peak near a time lag of 0 of the data is beyond random coincidence and that the two light curves are indeed correlated with a near 0 offset in time. Furthermore, the flux correlation factor of the X-ray to Gamma Ray, and X-ray to TeV for Mrk 421 falls out of the two-sigma range, suggesting a strong correlation. The best representations of the data are of the X-ray to TeV data because they represent similar regions of their respective 'humps' in the spectral energy distribution, and changes in the flux are more apparent in the X-ray and TeV regime. This data supports the hypothesis proposed by the Synchrotron Self-Compton model, where the photons produced by the synchrotron radiation are immediately available to be then scattered to a higher photon energy through Inverse Compton scattering. This is consistent with the physical structure of our targets, both are BL Lac objects whose spectral profile has no emission lines. Emission lines indicate that there are clouds of gas near the black hole absorbing and re-radiating energy from the jet and thermal excitation from accretion. The absence of the external clouds that would produce such emission lines would further support the prevailing theory that the TeV energy photons are caused not by External Compton (which would require some external cloud structure producing photons in most models), but by Synchrotron Self-Compton.

References

[1] Abdo A. A. et al. ApJ, 736, 131 (2011)

[2] Acciari, V. A. et al. ApJ, 679, 1427 (2008)

[3] Atwood, W. B., et al. ApJ, 697, 1071 (2009)

[4] Boettcher, M. Invited Review at "The Multimessenger Approach to Gamma-Ray Sources", astro-ph/0608713, (2006)

[5] Edelson, R. A. & Krolik, J. H. ApJ, 333, 646 (1988)

[6] Fossati, G. et al. ApJ, 677, 906 (2008)

[7] Punch, M. et al., Nature, 358, 477 (1992)

[8] Schubnell, M. S. et al. ApJ, 460, 644S (1996)

[9] Takahashi, T. ApJ, 470, 89 (1996)

[10] Timmer, J. & Konig, M., A\&A, 300, 707 (1995)

[11] Urry C. M., Padovani, P. PASP, 107, 83 (1995)

[12] Uttley, P., Mc Hardy, I. M., & Papadakis, I. E., MNRAS, 332, 231 (2002)